

# A critical nematic phase with pseudogap-like behavior in twisted bilayers

Virginia Gali, Matthias Hecker, and Rafael M. Fernandes

School of Physics and Astronomy, University of Minnesota, Minneapolis 55455 MN, USA

(Dated: January 4, 2024)

The crystallographic restriction theorem constrains two-dimensional nematicity to display either Ising ( $Z_2$ ) or three-state-Potts ( $Z_3$ ) critical behaviors, both of which are dominated by amplitude fluctuations. Here, we use group theory and microscopic modeling to show that this constraint is circumvented in a  $30^\circ$ -twisted hexagonal bilayer due to its emergent quasicrystalline symmetries. We find a critical phase dominated by phase fluctuations of a  $Z_6$  nematic order parameter and bounded by two Berezinskii-Kosterlitz-Thouless (BKT) transitions, which displays only quasi-long-range nematic order. The electronic spectrum in the critical phase displays a thermal pseudogap-like behavior, whose properties depend on the anomalous critical exponent. We also show that an out-of-plane magnetic field induces nematic phase fluctuations that suppress the two BKT transitions via a mechanism analogous to the Hall viscoelastic response of the lattice, giving rise to a putative nematic quantum critical point with emergent continuous symmetry. Finally, we demonstrate that even in the case of an untwisted bilayer, a critical phase emerges when the nematic order parameter changes sign between the two layers, establishing an odd-parity nematic state.

The discovery of magic-angle twisted bilayer graphene [1–5] heralded the field of twistronics, enabled by the remarkable precision with which twist angles can be tuned [6–10]. By imposing an underlying superlattice potential on the charge carriers [11], twisting affects the electronic properties of 2D systems in various ways. Besides the emergence of flat bands from the band folding reconstruction at magic twist angles [12], the superlattice, being an incommensurate array of registered sites, displays features with no counterpart on crystalline lattices that significantly affect the electronic degrees of freedom. Indeed, for small twist angles, the elastic excitations of the resulting moiré superlattice behave very differently from standard acoustic phonons [13–17], thus influencing transport properties [18, 19] and possibly superconductivity [20, 21]. Conversely, for certain large twist angles, the twisted superlattice acquires symmetries forbidden by the crystallographic restriction theorem, which enables new electronically ordered states [22, 23]. For instance, the superlattice formed by twisting two tetragonal layers by  $45^\circ$  has an eight-fold improper rotational symmetry [24]. In the presence of  $d$ -wave pairing interactions, this symmetry enforces the superconducting state to be the exotic  $d+id$  [25], as recently proposed to be realized in twisted cuprates [25–33].

Besides superconductivity, another electronic state strongly affected by the symmetries of the underlying lattice is the electronic nematic [34], in which electron-electron interactions lead to the spontaneous breaking of rotational symmetry [35, 36]. In 2D isotropic space, this is a continuous  $U(1)$  (or XY) symmetry that, when broken, triggers a nematic Goldstone mode that couples directly to the electronic charge density – unlike magnon or phonon Goldstone modes – and promotes non-Fermi-liquid behavior at zero temperature [37, 38]. At nonzero temperatures, only quasi-long-range nematic order is allowed across a critical phase [Fig. 1(a)], whose impact on the electronic spectrum remains unexplored. These appealing features of the isotropic nematic, however, are not realized in 2D crystals, since the underlying lattice lowers the continuous rotational symmetry to  $Z_2$  (Ising, in tetragonal lattices) [35, 36]

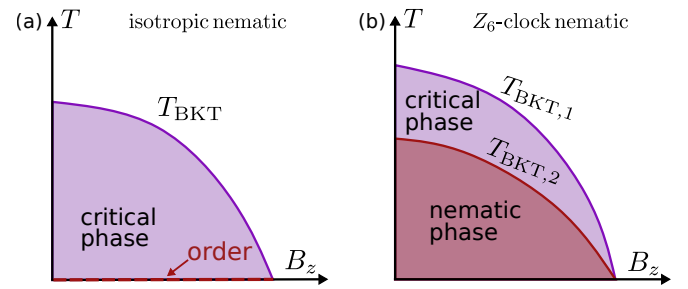


Figure 1. Schematic phase diagrams in 2D of (a) the isotropic nematic model and (b) the  $Z_6$ -clock nematic model realized on hexagonal layers twisted by  $30^\circ$ . While both feature a BKT transition towards a critical phase with quasi-long-range nematic order (purple), long-range order (red) is established at nonzero temperatures in the  $Z_6$  case via another BKT transition and only at  $T = 0$  in the isotropic case.  $B_z$  is an out-of-plane magnetic field.

or  $Z_3$  (3-state Potts/clock, in hexagonal lattices) [39–41].

Here, we show that these crystallographic restrictions on nematic phenomena are circumvented in hexagonal bilayers twisted by  $30^\circ$ , as the resulting twisted superlattice is a quasicrystal with a non-crystallographic twelve-fold improper rotation axis [42, 43]. Using group-theory and a microscopic model, we find that the nematic order parameter has the  $Z_6$  symmetry of a six-state clock model [44]. As a result, before the onset of long-range nematic order, the system displays a critical nematic phase with quasi-long-range order (like the isotropic nematic) bounded by two Berezinskii-Kosterlitz-Thouless (BKT) transitions, see Fig. 1(b).

Upon computing the electronic self-energy, we find that the nematic phase fluctuations inside the critical phase suppress the density of states (DOS) at the Fermi level and promote a pronounced peak in the spectral function at a frequency set by the anomalous exponent, a behavior reminiscent of a pseudogap. We also demonstrate that an out-of-plane magnetic field triggers fluctuations of the nematic phase via a mechanism analogous to the viscoelastic Hall response of the lattice [45–47]. Consequently, a magnetic field acts as an effective

transverse nematic field, driving the two BKT transitions towards a nematic quantum critical point (QCP) [Fig. 1(b)]. This QCP is expected to belong to the XY universality class and to trigger a pseudo-Goldstone mode, which can promote a non-Fermi-liquid to Fermi-liquid crossover at  $T = 0$  – similarly to the recently studied valley-polarized  $T = 0$  nematic state [48].

We start by considering two identical hexagonal layers, each with point group  $D_6$  and described by the non-interacting Hamiltonian  $\mathcal{H}_{0,\mu} = \sum_{\mathbf{k}} \mathbf{c}_{\mathbf{k},\mu}^\dagger \left( \varepsilon_{\mathbf{k}} + \delta_0 f_{\mathbf{k}}^{A_1} \right) \sigma^0 \mathbf{c}_{\mathbf{k},\mu}$ , with electronic operators  $\mathbf{c}_{\mathbf{k},\mu} \equiv (c_{\mathbf{k}\uparrow,\mu}, c_{\mathbf{k}\downarrow,\mu})$ , momentum  $\mathbf{k} = |\mathbf{k}|(\cos\theta, \sin\theta)$ , spin-space Pauli matrices  $\sigma^i$ , and layer index  $\mu = t, b$  for top and bottom layers, respectively. To keep the analysis general, the electronic dispersion consists of an isotropic term  $\varepsilon_{\mathbf{k}} = \frac{k^2}{2m} - \mu_0$  and a hexagonal warping term with coefficient  $\delta_0$  and form factor  $f_{\mathbf{k}}^{A_1} = \cos(6\theta)$ . The electronic nematic degrees of freedom are described by the two-component collective field  $\boldsymbol{\phi}_\mu = |\boldsymbol{\phi}_\mu|(\cos\alpha_\mu, \sin\alpha_\mu)$  that couples to the  $d_{x^2-y^2}$  and  $d_{xy}$  quadrupolar charge densities of each layer,  $\mathcal{H}_{\text{nem},\mu} = -g \sum_{\mathbf{k}} \mathbf{c}_{\mathbf{k},\mu}^\dagger \left( \boldsymbol{\phi}_\mu \cdot \mathbf{f}_{\mathbf{k}}^{E_2} \right) \sigma^0 \mathbf{c}_{\mathbf{k},\mu}$ , with form-factor  $\mathbf{f}_{\mathbf{k}}^{E_2} = (\cos 2\theta, -\sin 2\theta)$  and coupling constant  $g$  [40]. The nematic properties of an isolated layer can be obtained from the Landau free-energy  $\mathcal{F}[\boldsymbol{\phi}_\mu]$ , which we derive directly from the microscopic Hamiltonian  $\mathcal{H}_\mu \equiv \mathcal{H}_{0,\mu} + \mathcal{H}_{\text{nem},\mu}$  (details in the Supplementary Material (SM)):

$$\mathcal{F}[\boldsymbol{\phi}] = \mathcal{F}_0[|\boldsymbol{\phi}|^2] + \lambda_q |\boldsymbol{\phi}|^q \cos(q\alpha), \quad (1)$$

where  $\mathcal{F}_0$  depends only on the amplitude and we omitted the layer subscript  $\mu$ . In our case,  $q = 3$ , i.e. the nematic transition belongs to the 2D three-state Potts/clock universality class – recall that the  $Z_q$ -Potts and  $Z_q$ -clock models are equivalent for  $q = 3$ , but not  $q > 3$  [49]. This is a well-established result [39, 40, 50] that can also be derived from group-theory. Since  $\boldsymbol{\phi}_\mu$  transforms as the  $E_2$  irreducible representation (irrep) of the  $D_6$  group, the free energy must have a cubic invariant because the decomposition of the product  $E_2 \otimes E_2 \otimes E_2 = A_1 \oplus A_2 \oplus E_2$  contains a term that transforms as the trivial irrep  $A_1$ . More broadly, for any of the ten 2D crystallographic point groups that admit a non-trivial nematic order parameter, the nematic free energy must have the form of Eq. (1) with  $q = 2$  ( $Z_2$  Ising) or  $q = 3$  ( $Z_3$  Potts/clock). In either case, the phase  $\alpha_\mu$  is strongly constrained to discrete values and phase fluctuations do not play an important role, unlike the isotropic nematic case.

The situation changes when the two layers are coupled and twisted by an angle  $\theta_{\text{tw}}$ , since the system can acquire crystallographically-forbidden symmetries, thus enabling other  $q$  values in Eq. (1). Instead of  $\boldsymbol{\phi}_t$  and  $\boldsymbol{\phi}_b$ , we consider their symmetric and antisymmetric rotated combinations,  $\boldsymbol{\phi}_\pm = \frac{1}{2} [\mathcal{R}_z(-\theta_{\text{tw}})\boldsymbol{\phi}_b \pm \mathcal{R}_z(\theta_{\text{tw}})\boldsymbol{\phi}_t]$ , where  $\mathcal{R}_z(\theta)$  is the rotation matrix with respect to the  $z$ -axis. This change of basis is convenient because the nematic directors in the two layers are rotated against each other by the horizontal mirror

reflection  $\sigma_h$  (corresponding to switching the layer indices),  $\boldsymbol{\phi}_{b/t} \xrightarrow{\sigma_h} \mathcal{R}_z(\pm 2\theta_{\text{tw}})\boldsymbol{\phi}_{t/b}$ , implying that the combinations  $\boldsymbol{\phi}_\pm$  are eigenstates of  $\sigma_h$ ,  $\boldsymbol{\phi}_\pm \xrightarrow{\sigma_h} \pm \boldsymbol{\phi}_\pm$ . Note that  $\sigma_h$  does not necessarily leave the twisted bilayer invariant.

Consider first the untwisted case,  $\theta_{\text{tw}} = 0$  [Fig. 2(e)]. In this case, the reflection  $\sigma_h$  is a symmetry of the bilayer, such that its point group becomes  $D_{6h} = D_6 \times \{E, \sigma_h\}$  rather than  $D_6$  (here  $E$  denotes the identity operator). With  $\boldsymbol{\phi}_\pm$  being even/odd under  $\sigma_h$ , they transform respectively as the irreps  $E_{2g}$  and  $E_{2u}$  of  $D_{6h}$ . Thus,  $\boldsymbol{\phi}_+$  still behaves as a  $Z_3$  nematic order parameter with the free energy given by Eq. (1) with  $q = 3$ . In contrast, the threefold rotational-symmetry-breaking pattern due to  $\boldsymbol{\phi}_-$  changes sign between the two layers – hence we dub  $\boldsymbol{\phi}_-$  an odd-parity nematic order. Importantly, because  $\boldsymbol{\phi}_-$  is odd under  $\sigma_h$ , the cubic term in Eq. (1) is no longer allowed, and the leading anisotropic term is the  $q = 6$  one.

We now twist the layers by  $\theta_{\text{tw}} = \pi/6$ . The resulting twisted lattice, shown in Fig. 2(b), is not invariant under  $\sigma_h$  but it is symmetric under an improper rotation  $S_{12} = \sigma_h C_{12z}$ , i.e. a twelve-fold rotation followed by a reflection, an operation that is forbidden in periodic crystals. Thus, the  $30^\circ$ -twisted bilayer is actually an aperiodic quasicrystal described by the non-crystallographic point group  $D_{6d} = D_6 \times \{E, S_{12}\}$  [42, 43], see also Fig. S1 in the SM. This construction, which was previously proposed to realize  $f + if$  and  $g + ig$  superconductivity [22, 23], is analogous to the  $45^\circ$ -twisted tetragonal bilayer, characterized by a non-crystallographic  $D_{4d}$  point group that enables  $d + id$  superconductivity [25].

For the  $30^\circ$ -twisted bilayer,  $\boldsymbol{\phi}_+$ , corresponding to pure nematic order, transforms as the  $E_2$  irrep of  $D_{6d}$ , whereas the odd-parity nematic  $\boldsymbol{\phi}_-$  transforms as  $E_4$ . Importantly, the combinations  $\boldsymbol{\phi}_+$ ,  $\boldsymbol{\phi}_-$  are odd/even under another symmetry operation of the twisted bilayer: the four-fold improper rotation  $S_4 = \sigma_h C_{4z}$ ,  $\boldsymbol{\phi}_\pm \xrightarrow{S_4} \mp \boldsymbol{\phi}_\pm$ . Consequently, the cubic term  $q = 3$  in the free energy (1) is forbidden for  $\boldsymbol{\phi}_+$ , and the leading-order anisotropy term is the  $q = 6$  one, which corresponds to the 2D six-state ( $Z_6$ ) clock model [44]. The resulting phase diagram, shown schematically in Fig. 1(b), displays two BKT phase transitions [44, 50–52]. Below  $T_{\text{BKT},1}$ , vortices and antivortices associated with the nematic phase  $\alpha_+$  bind into pairs, like in the XY model. Below  $T_{\text{BKT},2}$ , the discrete nature of  $\alpha_+$  becomes relevant and long-range nematic order emerges. Thus, for  $T_{\text{BKT},2} \leq T \leq T_{\text{BKT},1}$  the system displays a critical phase with quasi-long-range nematic order. Remarkably, the quasicrystalline symmetry of the  $30^\circ$ -twisted bilayer enables the system to display the same behavior as that of the isotropic (XY) nematic phase over a wide temperature range.

We now show that the same results obtained using group-theory follow from the microscopic model. Upon coupling the two layers via a simple tunneling Hamiltonian [25],  $\mathcal{H}_{b-t} = t \sum_{\mathbf{k}} \mathbf{c}_{\mathbf{k},t}^\dagger \sigma^0 \mathbf{c}_{\mathbf{k},b} + \text{h.c.}$ , and rotating the top/bottom layer by  $\pm\theta_{\text{tw}}/2$ , respectively, we obtain  $\mathcal{H}_{\text{tot}} = \mathcal{H}_b + \mathcal{H}_t + \mathcal{H}_{b-t}$ :

$$\mathcal{H}_{\text{tot}} = \sum_{\mathbf{k}} \mathbf{c}_{\mathbf{k}}^\dagger \left\{ \varepsilon_{\mathbf{k}} \tau^0 + \delta_0 f_{\mathbf{k}}^{A_1} \cos(3\theta_{\text{tw}}) \tau^0 + \delta_0 f_{\mathbf{k}}^{A_2} \sin(3\theta_{\text{tw}}) \tau^z - g \left( \phi_+ \cdot f_{\mathbf{k}}^{E_2} \tau^0 + \phi_- \cdot f_{\mathbf{k}}^{E_2} \tau^z \right) + t \tau^x \right\} \sigma^0 \mathbf{c}_{\mathbf{k}}, \quad (2)$$

where  $\mathbf{c}_{\mathbf{k}} = (\mathbf{c}_{\mathbf{k},b}, \mathbf{c}_{\mathbf{k},t})$ ,  $f_{\mathbf{k}}^{A_2} = \sin(6\theta)$ , and  $\tau^i$  are layer-space Pauli matrices. The free energy of this model,  $\mathcal{F}[\phi_+, \phi_-]$ , is derived in the SM. Regardless of  $\theta_{\text{tw}}$ , the ‘‘pure’’ nematic order parameter  $\phi_+$  and  $\phi_-$  decouple to quadratic order, although  $\theta_{\text{tw}}$  affects their higher-order couplings (see SM). Most importantly, there is always a  $q = 3$  cubic term for both  $\phi_+$  and  $\phi_-$ , except when  $\theta_{\text{tw}} = \pi/6$  ( $\theta_{\text{tw}} = 0$ ), in which case the cubic term vanishes for the pure nematic  $\phi_+$  (odd-parity nematic  $\phi_-$ ) and the corresponding free energy becomes that of Eq. (1) with  $q = 6$ .

We also diagonalize  $\mathcal{H}_{\text{tot}}$  to obtain the reconstructed Fermi surfaces (FS). Figs. 2(a),(d) show the FS in the disordered phase for the  $30^\circ$ -twisted ( $\theta_{\text{tw}} = \pi/6$ ) and untwisted ( $\theta_{\text{tw}} = 0$ ) cases. Despite the incommensurate nature of the twisted system for arbitrary  $\theta_{\text{tw}}$ , its FS can be represented in the untwisted Brillouin zone provided the tunneling  $t$  is small, in which case the main effect of the aperiodic potential is to split the crossings between the top- and bottom-layer FS [22], as highlighted by the color coding in the figure. A similar approach is often employed for incommensurate charge density-waves [53] and magic-angle TBG, whose moiré superlattice is also incommensurate [10]. In Figs. 2(c),(f) we show the impact on the FS of long-range nematic order  $\phi_+ = \phi_0(1, 0)$  in the twisted case and odd-parity nematic order  $\phi_- = \phi_0(1, 0)$  in the untwisted case, highlighting the threefold rotational-symmetry-breaking.

While below  $T_{\text{BKT},2}$  the electronic spectrum is determined by  $\phi_{\pm} \neq 0$ , as shown in Figs. 2(c),(f), the spectrum inside the critical phase  $T_{\text{BKT},2} \leq T \leq T_{\text{BKT},1}$  is governed by phase fluctuations. To capture this effect, we compute the one-loop electronic self-energy  $\Sigma(\omega, \mathbf{k}) = g^2 A_0 T \sum_{i,j} \int_q \chi_{\text{nem}}^{ij}(\Omega, \mathbf{q}) f_{\mathbf{k}-\frac{\mathbf{q}}{2},i}^{E_2} f_{\mathbf{k}-\frac{\mathbf{q}}{2},j}^{E_2} \mathcal{G}(\omega - \Omega, \mathbf{k} - \mathbf{q})$ ,

where  $\chi_{\text{nem}}^{ij}$  is the nematic susceptibility,  $A_0$  is the area, and  $\mathcal{G}$  is the non-interacting Green’s function. While for the specific model considered above  $\mathcal{G}$  can be read off from Eq. (2), here we consider a generic linearized electronic dispersion. This enables us to extend the results to other systems that display a critical phase associated with a  $Z_6$  nematic-like order parameter, such as the odd-parity nematic order for  $\theta_{\text{tw}} = 0$  and the recently discussed spin-polarized [54–56] and valley-polarized [48, 50] nematic orders.

Inside the critical phase, the nematic susceptibility  $\chi_{\text{nem}}^{ij}(0, \mathbf{q}) = (|\mathbf{q}|/k_F)^{\eta-2} \chi_0 \delta_{ij}$  is characterized by the anomalous exponent  $\eta$ . Related to the phase-fluctuation stiffness  $\rho_s$  by  $\eta(T) = T/(2\pi\rho_s)$ ,  $\eta$  acquires the universal value  $\eta(T_{\text{BKT},1}) = 1/4$  at the upper BKT transition and decreases continuously until  $\eta(T_{\text{BKT},2}) = 1/9$  is reached at the lower BKT transition [44], where long-range nematic order onsets. Note that, since the critical phase occurs at finite temperatures, we set the frequency of the bosonic propagator to zero in our

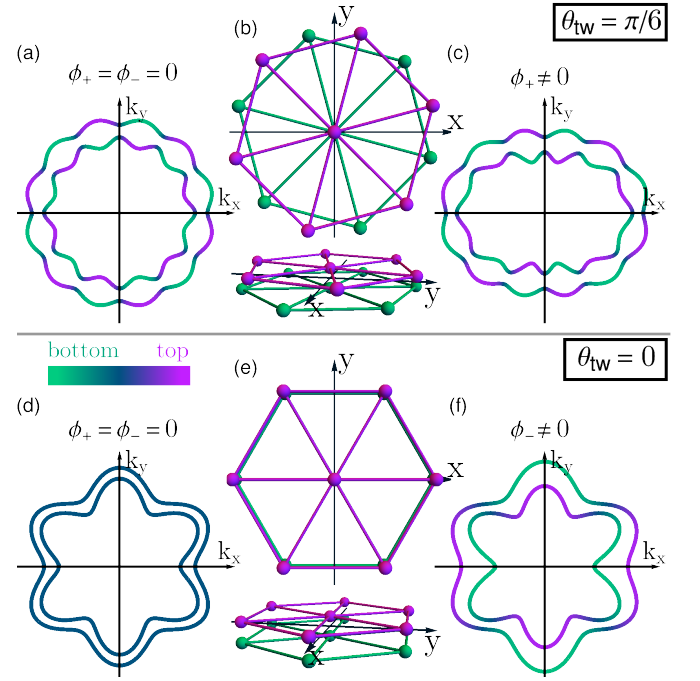


Figure 2.  $30^\circ$ -twisted [(a)-(c)] and untwisted [(d)-(f)] hexagonal bilayer system. In each case we show the lattice structure [(b), (e)], the FS without nematic order [(a), (d)], and the FS in the presence of pure nematic (c) or odd-parity nematic order (f). The color code denotes the spectral weight from the top and bottom layers.

calculation of the self-energy; such a quasistatic approximation is commonly employed to describe the effects of fluctuating order on the electronic spectrum at non-zero temperatures [57–59]. Moreover, we also introduce a quasiparticle lifetime  $\tau_0^{-1}$  to model the thermal broadening of the spectral function arising from correlations not associated with nematicity, such that  $\mathcal{G}^{-1} = \omega - \mathbf{v}_F \cdot \mathbf{q} + i\tau_0^{-1}/2$ , with Fermi velocity  $\mathbf{v}_F$ . Computing the one-loop self-energy at the Fermi momentum  $k_F$ , we find (see SM):

$$\Sigma(\omega, \mathbf{k}_F) = \kappa T c_\eta e^{-i\frac{\eta\pi}{2}} \left( \frac{2\omega\tau_0 + i}{2E_F\tau_0} \right)^{\eta-1}, \quad (3)$$

where  $c_\eta = \frac{\pi^{\frac{3}{2}} \Gamma(\frac{1}{2} - \frac{\eta}{2})}{2^{\eta} \Gamma(1 - \frac{\eta}{2})} \frac{1}{\sin(\frac{\eta\pi}{2})}$ ,  $E_F = \frac{v_F k_F}{2}$  is the Fermi energy, and  $\kappa = \frac{g^2 k_F^2 A \chi_0}{(2\pi)^2 E_F}$  is a dimensionless parameter. Fig. 3(a) shows the corresponding electronic spectral function  $A(\omega, \mathbf{k}_F) = -2\text{Im}[\hat{\mathcal{G}}(\omega, \mathbf{k}_F)]$ , with  $\hat{\mathcal{G}}^{-1} = \mathcal{G}^{-1} - \Sigma$ , for the values  $\eta$  assumes inside the critical phase,  $1/9 \leq \eta \leq 1/4$ . The spectral weight is strongly suppressed at the Fermi level and transferred to peaks at higher energies  $\pm\omega_{\text{peak}}$ , a behavior reminiscent of a pseudogap. As shown in Fig. 3(b), the pseudogap-like energy scale  $\Delta = 2\omega_{\text{peak}}$  increases with decreasing  $\eta$  and depends very weakly on the lifetime  $\tau_0$ , being well approximated by the  $\tau_0 \rightarrow \infty$  analytical expression:

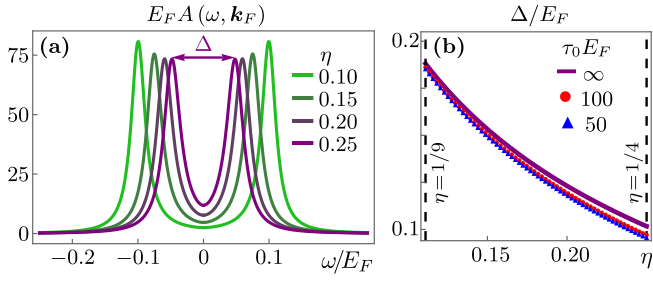


Figure 3. (a) The electronic spectral function  $A(\omega, \mathbf{k}_F)$  in the critical nematic phase for  $\eta$  within the range  $1/9 \leq \eta \leq 1/4$ ; here,  $T = 0.01E_F$  and  $\tau_0 = 50E_F^{-1}$ . (b) The pseudogap-like energy scale  $\Delta$  as a function of  $\eta$  for different lifetime values  $\tau_0$ . The solid line is the analytical result (4).

$$\Delta \approx 2E_F \left[ \frac{\kappa T}{E_F} \frac{a_\eta (1-2\eta)}{\eta+1} \left( \sqrt{1 + \frac{3c_\eta^2 (1-\eta^2)}{a_\eta^2 (1-2\eta)}} - 1 \right) \right]^{\frac{1}{2-\eta}} \quad (4)$$

where  $a_\eta \equiv c_\eta \cos(\frac{\eta\pi}{2})$ . We emphasize that  $\Delta \ll E_F$  within our weak-coupling approach. Moreover, as expected within a quasistatic approximation,  $\Delta$  is a purely thermal effect that would vanish as  $T \rightarrow 0$ , which is not reached here since long-range nematic order onsets at  $T_{\text{BKT},2}$ . The pseudogap-like behavior found here is qualitatively different from previously studied mechanisms [57, 58, 60–63], as it arises entirely from the nematic phase fluctuations in the critical phase. Nevertheless, it is interesting to note that finite-energy peaks in the spectral function were also obtained in Ref. [64], which included the anomalous exponent in their model of pairing phase fluctuations.

The behaviors discussed so far occur at finite temperatures. This motivates us to ask if a tuning parameter can suppress the BKT transitions and promote quantum critical fluctuations. Using group-theory, we find that an out-of-plane magnetic field  $B_z$  induces nematic phase fluctuations, via the following coupling in the nematic action  $\mathcal{S}[\phi_+] = \mathcal{F}[\phi_+]/T$ :

$$\mathcal{S}[\phi_+] = \lambda B_z \int_r (\phi_+ i \rho^y \dot{\phi}_+) = \lambda B_z \int_r |\phi_+(r)|^2 \frac{d\alpha_+(r)}{dt} \quad (5)$$

where  $r = (\mathbf{r}, t)$ ,  $\lambda$  is a coupling constant, and  $\rho^i$  are nematic-space Pauli matrices. Thus,  $B_z$  acts similarly to a transverse field to the emergent XY nematic order parameter, which is expected to suppress nematic order. This term is the nematic analogue of the (non-dissipative) viscoelastic response of a hexagonal lattice, by which external shear stress  $\sigma_{xy}$  induces a time-changing transverse strain  $\epsilon_{x^2-y^2}$  via  $\sigma_{xy} = \eta_H \frac{d\epsilon_{x^2-y^2}}{dt}$  [65–67]. Therefore,  $\lambda B_z$  plays a similar role as the Hall viscosity coefficient  $\eta_H$ . Interestingly, a term analogous to Eq. (5) was shown to emerge in nematic quantum Hall states as a result of the explicitly broken time-reversal symmetry [45–47].

The  $(B_z, T)$  nematic phase diagram of the 30°-twisted bilayer should then be similar to the phase diagram of the quan-

tum six-state clock model previously investigated in other contexts [50–52], as schematically shown in Fig. 1(b). Because at  $T = 0$  the system is above the upper critical dimension  $d_u \lesssim 3$  of the  $Z_6$ -clock model, the coefficient of the  $q = 6$  term in the free energy (1) is dangerously irrelevant, resulting in an XY nematic QCP and in a pseudo-Goldstone mode inside the  $T = 0$  nematically ordered state [68, 69]. As discussed in Ref. [48], its coupling to the low-energy electronic states results in a crossover from non-Fermi-liquid to Fermi-liquid behavior. An interesting question is how the system interpolates between the pseudogap-like behavior in the critical phase ( $T_{\text{BKT},2} \leq T \leq T_{\text{BKT},1}$ ) and the non-Fermi-liquid to Fermi-liquid crossover at  $T = 0$  as  $T_{\text{BKT},i} \rightarrow 0$ . Addressing this question will require incorporating nematic temporal fluctuations, which is beyond the scope of this work.

In summary, we established the nematic phase diagram of the 30°-twisted hexagonal bilayer. Its non-crystallographic symmetries endow nematicity with an enhanced  $Z_6$ -clock symmetry that is forbidden in any 2D crystalline system, leading to a critical phase displaying quasi-long-range nematic order over an extended temperature range. Phase fluctuations in this critical phase have a pronounced impact on the electronic spectrum, promoting a thermal pseudogap-like behavior. The two BKT transitions bounding the critical phase can be suppressed by a perpendicular magnetic field, which promotes quantum nematic phase fluctuations via a mechanism analogous to the Hall viscoelastic response of the lattice. An interesting direction is whether superconductivity emerges at this putative QCP. While it is well-established that Ising-nematic quantum critical fluctuations lead to enhanced pairing [70, 71], the case of an emergent XY nematic demands further investigations.

Experimentally, 30°-twisted bilayer graphene has been realized [43]. However, nematic order has not yet been observed in graphene, although it is theoretically predicted to emerge at the van Hove filling [72, 73]; furthermore, nematic order has been experimentally reported in Bernal bilayer graphene [74]. Importantly, recent advances in twisting non van-der-Waals materials [8] suggest the potential feasibility of 30°-twisted bilayers of materials beyond graphene. In this regard, nematic order is observed in several compounds whose lattices have threefold rotational symmetry, such as doped  $\text{Bi}_2\text{Se}_3$  [75, 76], bismuth [77], intercalated  $\text{Fe}_{1/3}\text{NbS}_2$  [78, 79] and the transition metal phosphorous trichalcogenides  $\text{MPX}_3$  which, by virtue of their van der Waals bonding, can be grown in few-layer form [80–83]. Besides crystals,  $Z_3$ -Potts nematicity has been observed in optical lattices [84], which are also amenable to twisting [85]. We emphasize that our analysis shows that the critical  $Z_6$  nematic phase emerges not only when the twist angle of the hexagonal bilayer is 30°, but even in the untwisted case, provided that the nematic order parameter changes sign between the two layers. Such an odd-parity nematic order is the counterpart of the time-reversal-odd spin- and valley-polarized nematic orders [48, 50, 54–56]. The latter, proposed to emerge in threefold symmetric systems near van Hove fillings, including twisted bilayer graphene, should also support a critical nematic phase that displays pseudogap-like behavior.

We thank A. Chubukov, I. Mandal, J. Schmalian, C. Xu for fruitful discussions. This work was supported by the U.S. Department of Energy, Office of Science, Basic Energy Sciences, Materials Sciences and Engineering Division, under Award No. DE-SC0020045.

- 
- [1] Y. Cao, V. Fatemi, S. Fang, K. Watanabe, T. Taniguchi, E. Kaxiras, and P. Jarillo-Herrero, *Unconventional superconductivity in magic-angle graphene superlattices*, *Nature* **556**, 43 (2018).
- [2] Y. Cao, V. Fatemi, A. Demir, S. Fang, S. L. Tomarken, J. Y. Luo, J. D. Sanchez-Yamagishi, K. Watanabe, T. Taniguchi, E. Kaxiras, *et al.*, *Correlated insulator behaviour at half-filling in magic-angle graphene superlattices*, *Nature* **556**, 80 (2018).
- [3] M. Yankowitz, S. Chen, H. Polshyn, Y. Zhang, K. Watanabe, T. Taniguchi, D. Graf, A. F. Young, and C. R. Dean, *Tuning superconductivity in twisted bilayer graphene*, *Science* **363**, 1059 (2019).
- [4] A. L. Sharpe, E. J. Fox, A. W. Barnard, J. Finney, K. Watanabe, T. Taniguchi, M. Kastner, and D. Goldhaber-Gordon, *Emergent ferromagnetism near three-quarters filling in twisted bilayer graphene*, *Science* **365**, 605 (2019).
- [5] X. Lu, P. Stepanov, W. Yang, M. Xie, M. A. Aamir, I. Das, C. Urgell, K. Watanabe, T. Taniguchi, G. Zhang, *et al.*, *Superconductors, orbital magnets and correlated states in magic-angle bilayer graphene*, *Nature* **574**, 653 (2019).
- [6] D. M. Kennes, M. Claassen, L. Xian, A. Georges, A. J. Millis, J. Hone, C. R. Dean, D. Basov, A. N. Pasupathy, and A. Rubio, *Moiré heterostructures as a condensed-matter quantum simulator*, *Nature Physics* **17**, 155 (2021).
- [7] K. F. Mak and J. Shan, *Semiconductor moiré materials*, *Nature Nanotechnology* **17**, 686 (2022).
- [8] J. Shen, Z. Dong, M. Qi, Y. Zhang, C. Zhu, Z. Wu, and D. Li, *Observation of Moiré Patterns in Twisted Stacks of Bilayer Perovskite Oxide Nanomembranes with Various Lattice Symmetries*, *ACS Applied Materials & Interfaces* **14**, 50386 (2022).
- [9] Y. Zhang, R. Polski, C. Lewandowski, A. Thomson, Y. Peng, Y. Choi, H. Kim, K. Watanabe, T. Taniguchi, J. Alicea, *et al.*, *Promotion of superconductivity in magic-angle graphene multilayers*, *Science* **377**, 1538 (2022).
- [10] A. Uri, S. C. de la Barrera, M. T. Randeria, D. Rodan-Legrain, T. Devakul, P. J. D. Crowley, N. Paul, K. Watanabe, T. Taniguchi, R. Lifshitz, L. Fu, R. C. Ashoori, and P. Jarillo-Herrero, *Superconductivity and strong interactions in a tunable moiré quasicrystal*, *Nature (London)* **620**, 762 (2023).
- [11] S. A. A. Ghorashi, A. Dunbrack, A. Abouelkomsan, J. Sun, X. Du, and J. Cano, *Topological and Stacked Flat Bands in Bilayer Graphene with a Superlattice Potential*, *Phys. Rev. Lett.* **130**, 196201 (2023).
- [12] R. Bistritzer and A. H. MacDonald, *Moiré bands in twisted double-layer graphene*, *Proceedings of the National Academy of Sciences* **108**, 12233 (2011).
- [13] M. Koshino and Y.-W. Son, *Moiré phonons in twisted bilayer graphene*, *Phys. Rev. B* **100**, 075416 (2019).
- [14] H. Ochoa, *Moiré-pattern fluctuations and electron-phason coupling in twisted bilayer graphene*, *Phys. Rev. B* **100**, 155426 (2019).
- [15] H. Ochoa and R. M. Fernandes, *Degradation of Phonons in Disordered Moiré Superlattices*, *Phys. Rev. Lett.* **128**, 065901 (2022).
- [16] Q. Gao and E. Khalaf, *Symmetry origin of lattice vibration modes in twisted multilayer graphene: Phasons versus moiré phonons*, *Phys. Rev. B* **106**, 075420 (2022).
- [17] R. Samajdar, Y. Teng, and M. S. Scheurer, *Moiré phonons and impact of electronic symmetry breaking in twisted trilayer graphene*, *Phys. Rev. B* **106**, L201403 (2022).
- [18] H. Ochoa and R. M. Fernandes, *Extended linear-in-T resistivity due to electron-phason scattering in moiré superlattices*, *Phys. Rev. B* **108**, 075168 (2023).
- [19] H. Ishizuka, A. Fahimniya, F. Guinea, and L. Levitov, *Purcell-like Enhancement of Electron-Phonon Interactions in Long-Period Superlattices: Linear-Temperature Resistivity and Cooling Power*, *Nano Letters* **21**, 7465 (2021).
- [20] F. Wu, E. Hwang, and S. Das Sarma, *Phonon-induced giant linear-in-T resistivity in magic angle twisted bilayer graphene: Ordinary strangeness and exotic superconductivity*, *Phys. Rev. B* **99**, 165112 (2019).
- [21] B. Lian, Z. Wang, and B. A. Bernevig, *Twisted Bilayer Graphene: A Phonon-Driven Superconductor*, *Phys. Rev. Lett.* **122**, 257002 (2019).
- [22] Y.-B. Liu, J. Zhou, Y. Zhang, W.-Q. Chen, and F. Yang, *Making chiral topological superconductors from nontopological superconductors through large angle twists*, *Phys. Rev. B* **108**, 064508 (2023).
- [23] Y.-B. Liu, Y. Zhang, W.-Q. Chen, and F. Yang, *High-angular-momentum topological superconductivities in twisted bilayer quasicrystal systems*, *Phys. Rev. B* **107**, 014501 (2023).
- [24] R. Haenel, T. Tummuru, and M. Franz, *Incoherent tunneling and topological superconductivity in twisted cuprate bilayers*, *Phys. Rev. B* **106**, 104505 (2022).
- [25] O. Can, T. Tummuru, R. P. Day, I. Elfmov, A. Damascelli, and M. Franz, *High-temperature topological superconductivity in twisted double-layer copper oxides*, *Nature Physics* **17**, 519 (2021).
- [26] T. Tummuru, E. Lantagne-Hurtubise, and M. Franz, *Twisted multilayer nodal superconductors*, *Phys. Rev. B* **106**, 014520 (2022).
- [27] X.-Y. Song, Y.-H. Zhang, and A. Vishwanath, *Doping a moiré Mott insulator: A  $t - J$  model study of twisted cuprates*, *Phys. Rev. B* **105**, L201102 (2022).
- [28] Y.-B. Liu, J. Zhou, C. Wu, and F. Yang, *Charge-4e superconductivity and chiral metal in  $45^\circ$ -twisted bilayer cuprates and related bilayers*, *Nature Communications* **14**, 7926 (2023).
- [29] P. A. Volkov, J. H. Wilson, K. P. Lucht, and J. H. Pixley, *Current- and Field-Induced Topology in Twisted Nodal Superconductors*, *Phys. Rev. Lett.* **130**, 186001 (2023).
- [30] P. A. Volkov, J. H. Wilson, K. P. Lucht, and J. H. Pixley, *Magic angles and correlations in twisted nodal superconductors*, *Phys. Rev. B* **107**, 174506 (2023).
- [31] A. C. Yuan, Y. Vituri, E. Berg, B. Spivak, and S. A. Kivelson, *Inhomogeneity-induced time-reversal symmetry breaking in cuprate twist junctions*, *Phys. Rev. B* **108**, L100505 (2023).
- [32] H. Wang, Y. Zhu, Z. Bai, Z. Wang, S. Hu, H.-Y. Xie, X. Hu, J. Cui, M. Huang, J. Chen, *et al.*, *Prominent Josephson tunneling between twisted single copper oxide planes of  $\text{Bi}_2\text{Sr}_{2-x}\text{La}_x\text{CuO}_{6+y}$* , *Nature Communications* **14**, 5201 (2023).
- [33] S. Y. F. Zhao, X. Cui, P. A. Volkov, H. Yoo, S. Lee, J. A. Gardener, A. J. Akey, R. Engelke, Y. Ronen, R. Zhong, G. Gu, S. Plugge, T. Tummuru, M. Kim, M. Franz, J. H. Pixley, N. Poccia, and P. Kim, *Time-reversal symmetry breaking superconductivity between twisted cuprate superconductors*, *Science*, eabl8371 (2023).
- [34] S. A. Kivelson, E. Fradkin, and V. J. Emery, *Electronic liquid-crystal phases of a doped Mott insulator*, *Nature* **393**, 550

- (1998).
- [35] E. Fradkin, S. A. Kivelson, M. J. Lawler, J. P. Eisenstein, and A. P. Mackenzie, *Nematic Fermi Fluids in Condensed Matter Physics*, *Annu. Rev. Condens. Matter Phys.* **1**, 153 (2010).
- [36] R. M. Fernandes, A. V. Chubukov, and J. Schmalian, *What drives nematic order in iron-based superconductors?*, *Nature Physics* **10**, 97 (2014).
- [37] V. Oganesyan, S. A. Kivelson, and E. Fradkin, *Quantum theory of a nematic Fermi fluid*, *Phys. Rev. B* **64**, 195109 (2001).
- [38] H. Watanabe and A. Vishwanath, *Criterion for stability of Goldstone modes and Fermi liquid behavior in a metal with broken symmetry*, *Proceedings of the National Academy of Sciences* **111**, 16314 (2014).
- [39] M. Hecker and J. Schmalian, *Vestigial nematic order and superconductivity in the doped topological insulator  $Cu_xBi_2Se_3$* , *npj Quantum Materials* **3**, 26 (2018).
- [40] R. M. Fernandes and J. W. Venderbos, *Nematicity with a twist: Rotational symmetry breaking in a moiré superlattice*, *Science Advances* **6**, eaba8834 (2020).
- [41] A. R. Chakraborty and R. M. Fernandes, *Strain-tuned quantum criticality in electronic Potts-nematic systems*, *Phys. Rev. B* **107**, 195136 (2023).
- [42] P. Stampfli, *A dodecagonal quasiperiodic lattice in two dimensions*, *Helv. Phys. Acta* **59**, 1260 (1986).
- [43] S. J. Ahn, P. Moon, T.-H. Kim, H.-W. Kim, H.-C. Shin, E. H. Kim, H. W. Cha, S.-J. Kahng, P. Kim, M. Koshino, *et al.*, *Dirac electrons in a dodecagonal graphene quasicrystal*, *Science* **361**, 782 (2018).
- [44] J. V. José, L. P. Kadanoff, S. Kirkpatrick, and D. R. Nelson, *Renormalization, vortices, and symmetry-breaking perturbations in the two-dimensional planar model*, *Phys. Rev. B* **16**, 1217 (1977).
- [45] J. Maciejko, B. Hsu, S. A. Kivelson, Y. Park, and S. L. Sondhi, *Field theory of the quantum Hall nematic transition*, *Phys. Rev. B* **88**, 125137 (2013).
- [46] Y. You and E. Fradkin, *Field theory of nematicity in the spontaneous quantum anomalous Hall effect*, *Phys. Rev. B* **88**, 235124 (2013).
- [47] Y. You, G. Y. Cho, and E. Fradkin, *Theory of Nematic Fractional Quantum Hall States*, *Phys. Rev. X* **4**, 041050 (2014).
- [48] I. Mandal and R. M. Fernandes, *Valley-polarized nematic order in twisted moiré systems: In-plane orbital magnetism and crossover from non-Fermi liquid to Fermi liquid*, *Phys. Rev. B* **107**, 125142 (2023).
- [49] F. Y. Wu, *The Potts model*, *Rev. Mod. Phys.* **54**, 235 (1982).
- [50] Y. Xu, X.-C. Wu, C.-M. Jian, and C. Xu, *Orbital order and possible non-Fermi liquid in moiré systems*, *Phys. Rev. B* **101**, 205426 (2020).
- [51] D. Podolsky, E. Shimshoni, G. Morigi, and S. Fishman, *Buckling Transitions and Clock Order of Two-Dimensional Coulomb Crystals*, *Phys. Rev. X* **6**, 031025 (2016).
- [52] M. Arnold and R. Nigmatullin, *Dynamics of vortex defect formation in two-dimensional Coulomb crystals*, *Phys. Rev. B* **106**, 104106 (2022).
- [53] M. R. Norman, A. Kanigel, M. Randeria, U. Chatterjee, and J. C. Campuzano, *Modeling the Fermi arc in underdoped cuprates*, *Phys. Rev. B* **76**, 174501 (2007).
- [54] C. Wu, K. Sun, E. Fradkin, and S.-C. Zhang, *Fermi liquid instabilities in the spin channel*, *Phys. Rev. B* **75**, 115103 (2007).
- [55] L. Classen, A. V. Chubukov, C. Honerkamp, and M. M. Scherer, *Competing orders at higher-order Van Hove points*, *Phys. Rev. B* **102**, 125141 (2020).
- [56] D. V. Chichinadze, L. Classen, and A. V. Chubukov, *Valley magnetism, nematicity, and density wave orders in twisted bilayer graphene*, *Phys. Rev. B* **102**, 125120 (2020).
- [57] J. Schmalian, D. Pines, and B. Stojković, *Weak pseudogap behavior in the underdoped cuprate superconductors*, *Phys. Rev. Lett.* **80**, 3839 (1998).
- [58] T. A. Sedrakyan and A. V. Chubukov, *Pseudogap in underdoped cuprates and spin-density-wave fluctuations*, *Phys. Rev. B* **81**, 174536 (2010).
- [59] J. Lin and A. J. Millis, *Optical and hall conductivities of a thermally disordered two-dimensional spin-density wave: Two-particle response in the pseudogap regime of electron-doped high- $T_c$  superconductors*, *Phys. Rev. B* **83**, 125108 (2011).
- [60] Y. M. Vilk and A.-M. S. Tremblay, *Destruction of Fermi-liquid quasiparticles in two dimensions by critical fluctuations*, *Europhysics Letters* **33**, 159 (1996).
- [61] M. R. Norman, M. Randeria, H. Ding, and J. C. Campuzano, *Phenomenology of the low-energy spectral function in high- $T_c$  superconductors*, *Phys. Rev. B* **57**, R11093 (1998).
- [62] M. Franz and A. J. Millis, *Phase fluctuations and spectral properties of underdoped cuprates*, *Phys. Rev. B* **58**, 14572 (1998).
- [63] S. Sachdev, H. D. Scammell, M. S. Scheurer, and G. Tarnopolsky, *Gauge theory for the cuprates near optimal doping*, *Phys. Rev. B* **99**, 054516 (2019).
- [64] S. Banerjee, T. V. Ramakrishnan, and C. Dasgupta, *Effect of pairing fluctuations on low-energy electronic spectra in cuprate superconductors*, *Phys. Rev. B* **84**, 144525 (2011).
- [65] B. Bradlyn, M. Goldstein, and N. Read, *Kubo formulas for viscosity: Hall viscosity, Ward identities, and the relation with conductivity*, *Phys. Rev. B* **86**, 245309 (2012).
- [66] M. Barkeshli, S. B. Chung, and X.-L. Qi, *Dissipationless phonon Hall viscosity*, *Phys. Rev. B* **85**, 245107 (2012).
- [67] J. M. Link, D. E. Sheehy, B. N. Narozhny, and J. Schmalian, *Elastic response of the electron fluid in intrinsic graphene: The collisionless regime*, *Phys. Rev. B* **98**, 195103 (2018).
- [68] M. Oshikawa, *Ordered phase and scaling in  $Z_n$  models and the three-state antiferromagnetic Potts model in three dimensions*, *Phys. Rev. B* **61**, 3430 (2000).
- [69] P. Patil, H. Shao, and A. W. Sandvik, *Unconventional  $U(1)$  to  $Z_q$  crossover in quantum and classical  $q$ -state clock models*, *Phys. Rev. B* **103**, 054418 (2021).
- [70] S. Lederer, Y. Schattner, E. Berg, and S. A. Kivelson, *Superconductivity and non-Fermi liquid behavior near a nematic quantum critical point*, *Proceedings of the National Academy of Sciences* **114**, 4905 (2017).
- [71] A. Klein and A. Chubukov, *Superconductivity near a nematic quantum critical point: Interplay between hot and lukewarm regions*, *Phys. Rev. B* **98**, 220501 (2018).
- [72] B. Valenzuela and M. A. Vozmediano, *Pomeranchuk instability in doped graphene*, *New Journal of Physics* **10**, 113009 (2008).
- [73] M. L. Kiesel, C. Platt, and R. Thomale, *Unconventional Fermi Surface Instabilities in the Kagome Hubbard Model*, *Phys. Rev. Lett.* **110**, 126405 (2013).
- [74] A. Mayorov, D. Elias, M. Mucha-Kruczynski, R. Gorbachev, T. Tudorovskiy, A. Zhukov, S. Morozov, M. Katsnelson, V. F. Ko, A. Geim, *et al.*, *Interaction-driven spectrum reconstruction in bilayer graphene*, *Science* **333**, 860 (2011).
- [75] Y. Sun, S. Kittaka, T. Sakakibara, K. Machida, J. Wang, J. Wen, X. Xing, Z. Shi, and T. Tamegai, *Quasiparticle Evidence for the Nematic State above  $T_c$  in  $Sr_xBi_2Se_3$* , *Phys. Rev. Lett.* **123**, 027002 (2019).
- [76] C.-w. Cho, J. Shen, J. Lyu, O. Atanov, Q. Chen, S. H. Lee, Y. S. Hor, D. J. Gawryluk, E. Pomjakushina, M. Bartkowiak, *et al.*,  *$Z_3$ -vestigial nematic order due to superconducting fluctuations in the doped topological insulators  $Nb_xBi_2Se_3$  and  $Cu_xBi_2Se_3$* , *Nature Communications* **11**, 3056 (2020).

- [77] B. E. Feldman, M. T. Randeria, A. Gyenis, F. Wu, H. Ji, R. J. Cava, A. H. MacDonald, and A. Yazdani, *Observation of a nematic quantum Hall liquid on the surface of bismuth*, [\*Science\* \*\*354\*\*, 316 \(2016\)](#).
- [78] A. Little, C. Lee, C. John, S. Doyle, E. Maniv, N. L. Nair, W. Chen, D. Rees, J. W. Venderbos, R. M. Fernandes, *et al.*, *Three-state nematicity in the triangular lattice antiferromagnet  $\text{Fe}_{1/3}\text{NbS}_2$* , [\*Nature materials\* \*\*19\*\*, 1062 \(2020\)](#).
- [79] S. C. Haley, S. F. Weber, T. Cookmeyer, D. E. Parker, E. Maniv, N. Maksimovic, C. John, S. Doyle, A. Maniv, S. K. Ramakrishna, A. P. Reyes, J. Singleton, J. E. Moore, J. B. Neaton, and J. G. Analytis, *Half-magnetization plateau and the origin of threefold symmetry breaking in an electrically switchable triangular antiferromagnet*, [\*Phys. Rev. Res.\* \*\*2\*\*, 043020 \(2020\)](#).
- [80] Z. Ni, D. S. Antonenko, W. J. Meese, Q. Tian, N. Huang, A. V. Haglund, M. Cothrine, D. G. Mandrus, R. M. Fernandes, J. W. Venderbos, *et al.*, *Signatures of  $Z_3$  Vestigial Potts-nematic order in van der Waals antiferromagnets*, [arXiv:2308.07249 \(2023\)](#).
- [81] K. Hwangbo, J. Cenker, E. Rosenberg, Q. Jiang, H. Wen, D. Xiao, J.-H. Chu, and X. Xu, *Strain Tuning Three-state Potts Nematicity in a Correlated Antiferromagnet*, [arXiv:2308.08734 \(2023\)](#).
- [82] Z. Sun, G. Ye, M. Huang, C. Zhou, N. Huang, Q. Li, Z. Ye, C. Nnokwe, H. Deng, D. Mandrus, *et al.*, *Dimensionality crossover to 2D vestigial nematicity from 3D zigzag antiferromagnetism in an XY-type honeycomb van der Waals magnet*, [arXiv:2311.03493 \(2023\)](#).
- [83] Q. Tan, C. A. Occhialini, H. Gao, J. Li, H. Kitadai, R. Comin, and X. Ling, *Revealing the three-state nematicity in atomically-thin antiferromagnetic  $\text{NiPS}_3$  via magneto-optical effect*, [arXiv:2311.12201 \(2023\)](#).
- [84] S. Jin, W. Zhang, X. Guo, X. Chen, X. Zhou, and X. Li, *Evidence of Potts-Nematic Superfluidity in a Hexagonal  $sp^2$  Optical Lattice*, [\*Phys. Rev. Lett.\* \*\*126\*\*, 035301 \(2021\)](#).
- [85] A. González-Tudela and J. I. Cirac, *Cold atoms in twisted-bilayer optical potentials*, [\*Phys. Rev. A\* \*\*100\*\*, 053604 \(2019\)](#).

# Supplementary Material: A critical nematic phase with pseudogap-like behavior in twisted bilayers

Virginia Gali, Matthias Hecker, and Rafael M. Fernandes

*School of Physics and Astronomy, University of Minnesota, Minneapolis, Minnesota 55455, USA*

## SI. FREE-ENERGY EXPANSION OF THE MODEL HAMILTONIAN

Here we provide details of the free energy expansion of the microscopic model introduced in the main text. We are interested in both the free energy  $\mathcal{F}[\phi_\mu]$  of a single layer, where  $\phi_\mu = (\phi_{\mu,1}, \phi_{\mu,2}) = |\phi_\mu|(\cos\alpha_\mu, \sin\alpha_\mu)$  is the collective nematic field in layer  $\mu$ , as well as the free energy  $\mathcal{F}[\phi_+, \phi_-]$  of the twisted bilayer system, where  $\phi_\pm = (\phi_{\pm,1}, \phi_{\pm,2}) = |\phi_\pm|(\cos\alpha_\pm, \sin\alpha_\pm)$ . For convenience, we first list the resulting free energy expansions and discuss their implications before delving into the details of the derivation. For the single layer, we find:

$$\mathcal{F}[\phi_\mu] = r|\phi_\mu|^2 + u|\phi_\mu|^4 + \lambda_3|\phi_\mu|^3 \cos(3\alpha_\mu), \quad (\text{S1})$$

which is identical to the  $Z_3$ -Potts model. For the twisted bilayer system with twist angle  $\theta_{\text{tw}}$ , on the other hand, the free energy is given by  $\mathcal{F}[\phi_+, \phi_-] = \mathcal{F}_+[\phi_+] + \mathcal{F}_-[\phi_-] + \mathcal{F}_m[\phi_\pm]$  with:

$$\begin{aligned} \mathcal{F}_+[\phi_+] &= \mathcal{F}_+^0[|\phi_+|] + \lambda_6^{(+)}|\phi_+|^6 \cos(6\alpha_+) \\ &+ |\phi_+|^3 \left\{ \lambda_+^{(3c)} + u_+^{(5)} \right\} |\phi_+|^2 \cos(3\theta_{\text{tw}}) \cos(3\alpha_+), \end{aligned} \quad (\text{S2})$$

$$\begin{aligned} \mathcal{F}_-[\phi_-] &= \mathcal{F}_-^0[|\phi_-|] + \lambda_6^{(-)}|\phi_-|^6 \cos(6\alpha_-) \\ &+ |\phi_-|^3 \left\{ \lambda_-^{(3s)} + u_-^{(5)} \right\} |\phi_-|^2 \sin(3\theta_{\text{tw}}) \sin(3\alpha_-), \end{aligned} \quad (\text{S3})$$

$$\begin{aligned} \mathcal{F}_m[\phi_\pm] &= 3\lambda_-^{(3c)} \cos(3\theta_{\text{tw}}) |\phi_+| |\phi_-|^2 \cos(2\alpha_- + \alpha_+) \\ &+ 3\lambda_-^{(3s)} \sin(3\theta_{\text{tw}}) |\phi_+|^2 |\phi_-| \sin(2\alpha_+ + \alpha_-) \\ &+ u_3 |\phi_+|^2 |\phi_-|^2 \{2 + \cos(2\alpha_+ - 2\alpha_-)\}. \end{aligned} \quad (\text{S4})$$

Here, we defined the term that depends only on the magnitude of the nematic order parameters as:

$$\mathcal{F}_\pm^0[|\phi|] = r_\pm |\phi|^2 + u_\pm |\phi|^4 + u_\pm^{(6)} |\phi|^6. \quad (\text{S5})$$

Importantly, in Eq. (S4), we note that there is no bilinear coupling between the two order parameter combinations. However, in cubic order, they have a linear-quadratic coupling in which one field acts as an external field to the other. In particular, a non-zero  $|\phi_-|$  induces  $|\phi_+| \sim \cos(3\theta_{\text{tw}}) |\phi_-|^2$  whereas a non-zero  $|\phi_+|$  induces  $|\phi_-| \sim \sin(3\theta_{\text{tw}}) |\phi_+|^2$ . Note that this type of linear-biquadratic coupling involving nematic order parameters is well understood and also emerges in the contexts of spin-polarized and valley-polarized nematics [48, 50, 56]. This means that, in the untwisted case ( $\theta_{\text{tw}} = 0$ ), the condensation of the odd-parity nematic order parameter  $|\phi_-|$  triggers also standard nematic order. Note that, depending on

the sign of  $\lambda_6^{(-)}$ ,  $\phi_-$  also triggers either an electric polarization  $P_z \propto |\phi_-|^3 \sin(3\alpha_-)$ , which transforms as the  $A_{2u}$  irrep of  $D_{6h}$ , or the  $l = 7$  electric multipole (octacosahexapole)  $\Upsilon_7 \propto |\phi_-|^3 \cos(3\alpha_-)$ , which transforms as  $A_{1u}$ . Conversely, in the  $30^\circ$ -twisted hexagonal bilayer ( $\theta_{\text{tw}} = \pi/6$ ), condensation of  $|\phi_+|$  also induces  $|\phi_-| \sim |\phi_+|^2$ . Moreover, analogously to  $\phi_-$  in the untwisted case,  $\phi_+$  induces, depending on the sign of  $\lambda_6^{(+)}$ , either the electric polarization  $P_z \propto |\phi_+|^3 \sin(3\alpha_+)$ , which transforms as  $B_2$  in  $D_{6d}$ , or the  $l = 6$  electric multipole (tetrahexacontapole)  $\Upsilon_6 \propto |\phi_+|^3 \cos(3\alpha_+)$ , which transforms as  $B_1$ .

From Eqs. (S2) and (S3), we conclude that unless the twist angle  $\theta_{\text{tw}} = n\frac{\pi}{6}$ , with  $n \in \mathbb{N}^0$ , the universality class of the nematic transition is  $Z_3$ -Potts. Only for  $\theta_{\text{tw}} = n\frac{\pi}{6}$  either  $\phi_+$  (when  $n$  is odd) or  $\phi_-$  (when  $n$  is even) acquires the more exotic  $Z_6$ -clock universality. Note that the linear-quadratic couplings only renormalize the quartic coefficient of the leading channel upon integrating out the fluctuations of the uncondensed order parameter. For the two specific twist angles studied in the main text, the above Landau expansions simplify to

$$\theta_{\text{tw}} = 0: \quad \mathcal{F}_+[\phi_+] = \mathcal{F}_+^0[|\phi_+|] + \lambda_+^{(3c)} |\phi_+|^3 \cos(3\alpha_+), \quad (\text{S6})$$

$$\mathcal{F}_-[\phi_-] = \mathcal{F}_-^0[|\phi_-|] + \lambda_6^{(-)} |\phi_-|^6 \cos(6\alpha_-), \quad (\text{S7})$$

and

$$\theta_{\text{tw}} = \frac{\pi}{6}: \quad \mathcal{F}_+[\phi_+] = \mathcal{F}_+^0[|\phi_+|] + \lambda_6^{(+)} |\phi_+|^6 \cos(6\alpha_+), \quad (\text{S8})$$

$$\mathcal{F}_-[\phi_-] = \mathcal{F}_-^0[|\phi_-|] + \lambda_+^{(3s)} |\phi_-|^3 \sin(3\alpha_-). \quad (\text{S9})$$

To emphasize that the  $30^\circ$ -twisted hexagonal bilayer system forms a quasi-crystalline pattern with no periodicity, we plot the corresponding arrangement of the sites of the top and bottom layers in Fig. S1.

To derive the Landau coefficients occurring in Eqs. (S1)-(S5), we start from the microscopic model Hamiltonian. Using the layer index  $\mu \in \{b, t\}$  for bottom and top layers, the single-layer nematic Hamiltonian is given by

$$\mathcal{H}_\mu = \sum_{\mathbf{k}} \mathbf{c}_{\mathbf{k},\mu}^\dagger \left\{ \left( \varepsilon_{\mathbf{k}} + \delta_0 f_{\mathbf{k}}^{A_1} \right) - g \left( \phi_\mu \cdot \mathbf{f}_{\mathbf{k}}^{E_2} \right) \right\} \sigma^0 \mathbf{c}_{\mathbf{k},\mu}, \quad (\text{S10})$$

with the electronic operator  $\mathbf{c}_{\mathbf{k},\mu} \equiv (c_{\mathbf{k}\uparrow,\mu}, c_{\mathbf{k}\downarrow,\mu})$ , the bare dispersion  $\varepsilon_{\mathbf{k}} = \frac{k^2}{2m} - \mu_0$  with momentum  $\mathbf{k} = (k_x, k_y) = |\mathbf{k}|(\cos\theta, \sin\theta)$  and chemical potential  $\mu_0$ . The two-component nematic order parameter in the  $(d_{x^2-y^2}, d_{xy})$ -symmetry channel is given by  $\phi_\mu = (\phi_{\mu,1}, \phi_{\mu,2})^T = |\phi_\mu| \mathbf{b}_{\alpha_\mu}$



where

$$\mathbf{b}_\alpha = (\cos \alpha, \sin \alpha)^T, \quad (\text{S11})$$

and  $g$  is the nematic coupling constant. The form factors are represented with respect to their transformation properties within the  $D_6$  point group, i.e. with respect to the corresponding irreducible representation (irrep). We define

$$f_k^{B_1} = \hat{k}_x^3 - 3\hat{k}_x\hat{k}_y^2 = \cos(3\theta), \quad (\text{S12})$$

$$f_k^{B_2} = \hat{k}_y^3 - 3\hat{k}_y\hat{k}_x^2 = -\sin(3\theta), \quad (\text{S13})$$

$$f_k^{A_1} = (f_k^{B_1})^2 - (f_k^{B_2})^2 = \cos(6\theta), \quad (\text{S14})$$

$$f_k^{A_2} = -2f_k^{B_1}f_k^{B_2} = \sin(6\theta), \quad (\text{S15})$$

$$f_k^{E_2} = \begin{pmatrix} \hat{k}_x^2 - \hat{k}_y^2 \\ -2\hat{k}_x\hat{k}_y \end{pmatrix} = \begin{pmatrix} \cos(2\theta) \\ -\sin(2\theta) \end{pmatrix}, \quad (\text{S16})$$

where  $\hat{\mathbf{k}} = \mathbf{k}/|\mathbf{k}|$ . Note that the symmetry elements of the  $D_6$  point group,

$$D_6 = \{E, C_{6z}^{\pm 1}, C_{3z}^{\pm 1}, C_{2z}\} \otimes \{E, C_{2x}\}, \quad (\text{S17})$$

are all preserved in the bilayer system regardless of the actual twist angle  $\theta_{\text{tw}}$ , cf. Fig. 2(b) of the main text. Correspondingly, any momentum summation where the argument does not transform trivially ( $A_1$ ) has to vanish for symmetry reasons, for example  $\sum_{\mathbf{k}} g_{\mathbf{k}}^{A_1} f_{\mathbf{k}}^{A_2} = 0$  where  $g_{\mathbf{k}}^{A_1}$  is an arbitrary function transforming as  $A_1$ .

As we couple the two layers (S10) by a tunneling Hamiltonian

$$\mathcal{H}_{b-t} = t \sum_{\mathbf{k}} \mathbf{c}_{\mathbf{k},t}^\dagger \sigma^0 \mathbf{c}_{\mathbf{k},b} + \text{h.c.}, \quad (\text{S18})$$

with tunneling amplitude  $t$ , we also rotate the bottom (top) layer by an angle  $-\theta_{\text{tw}}/2$  ( $+\theta_{\text{tw}}/2$ ). This rotation affects the form factors according to:

$$f_{\mathcal{R}_z(\pm\theta_{\text{tw}}/2)\mathbf{k}}^{E_2} = \mathcal{R}_z(\mp\theta_{\text{tw}}) f_{\mathbf{k}}^{E_2}, \quad (\text{S19})$$

$$f_{\mathcal{R}_z(\pm\theta_{\text{tw}}/2)\mathbf{k}}^{A_1} = f_{\mathbf{k}}^{A_1} \cos(3\theta_{\text{tw}}) \mp f_{\mathbf{k}}^{A_2} \sin(3\theta_{\text{tw}}), \quad (\text{S20})$$

with the rotation matrix

$$\mathcal{R}_z(\gamma) = \begin{pmatrix} \cos \gamma & -\sin \gamma \\ \sin \gamma & \cos \gamma \end{pmatrix}. \quad (\text{S21})$$

As a result, the total Hamiltonian  $\mathcal{H}_{\text{tot}} = \mathcal{H}_b + \mathcal{H}_t + \mathcal{H}_{b-t}$  becomes

$$\begin{aligned} \mathcal{H}_{\text{tot}} = \sum_{\mathbf{k}} \mathbf{c}_{\mathbf{k}}^\dagger \left\{ \left[ \varepsilon_{\mathbf{k}} + \delta_0 f_{\mathbf{k}}^{A_1} \cos(3\theta_{\text{tw}}) \right] \tau^0 + \delta_0 f_{\mathbf{k}}^{A_2} \sin(3\theta_{\text{tw}}) \tau^z \right. \\ \left. - g \left( \boldsymbol{\phi}_+ \cdot f_{\mathbf{k}}^{E_2} \tau^0 + \boldsymbol{\phi}_- \cdot f_{\mathbf{k}}^{E_2} \tau^z \right) + t \tau^x \right\} \sigma^0 \mathbf{c}_{\mathbf{k}}, \quad (\text{S22}) \end{aligned}$$

where  $\mathbf{c}_{\mathbf{k}} = (\mathbf{c}_{\mathbf{k},b}, \mathbf{c}_{\mathbf{k},t})$  denotes the four-component fermionic basis and  $\tau^i$  are Pauli matrices acting on the layer subspace. Here, we introduced the symmetrized and anti-symmetrized combinations of the nematic order parameters

$$\boldsymbol{\phi}_{\pm} = \frac{1}{2} \left( \mathcal{R}_z^T(\theta_{\text{tw}}) \boldsymbol{\phi}_b \pm \mathcal{R}_z(\theta_{\text{tw}}) \boldsymbol{\phi}_t \right). \quad (\text{S23})$$

As explained in the main text, only these combinations have a well-defined transformation behavior under the reflection symmetry operation  $\sigma_h$ , i.e.  $\boldsymbol{\phi}_{\pm} \xrightarrow{\sigma_h} \pm \boldsymbol{\phi}_{\pm}$  due to the individual transformation  $\boldsymbol{\phi}_{b/t} \xrightarrow{\sigma_h} \mathcal{R}_z(\pm 2\theta_{\text{tw}}) \boldsymbol{\phi}_{t/b}$ .

For later use, we will need the symmetry-decomposition of powers of  $(\hat{\boldsymbol{\phi}}_{\mu} \cdot f_{\mathbf{k}}^{E_2})^l$  where  $\hat{\boldsymbol{\phi}}_{\mu} = \boldsymbol{\phi}_{\mu}/|\boldsymbol{\phi}_{\mu}|$ . To do this, we introduce the higher-order form factors in the  $E_2$ -channel given by

$$f_{\mathbf{k}}^{2,E_2} = \begin{pmatrix} (f_{\mathbf{k},1}^{E_2})^2 - (f_{\mathbf{k},2}^{E_2})^2 \\ -2f_{\mathbf{k},1}^{E_2} f_{\mathbf{k},2}^{E_2} \end{pmatrix} = \begin{pmatrix} \cos(4\theta) \\ \sin(4\theta) \end{pmatrix}, \quad (\text{S24})$$

$$f_{\mathbf{k}}^{4,E_2} = \begin{pmatrix} (f_{\mathbf{k},1}^{2,E_2})^2 - (f_{\mathbf{k},2}^{2,E_2})^2 \\ -2f_{\mathbf{k},1}^{2,E_2} f_{\mathbf{k},2}^{2,E_2} \end{pmatrix} = \begin{pmatrix} \cos(8\theta) \\ -\sin(8\theta) \end{pmatrix}, \quad (\text{S25})$$

which allows us to compute the symmetry decompositions up to fourth order:

$$\begin{aligned} h_{\mu\nu,\mathbf{k}}^{(2)} &\equiv \left( \hat{\boldsymbol{\phi}}_{\mu} \cdot f_{\mathbf{k}}^{E_2} \right) \left( \hat{\boldsymbol{\phi}}_{\nu} \cdot f_{\mathbf{k}}^{E_2} \right) \\ &= \frac{1}{2} \cos(\alpha_{\mu} - \alpha_{\nu}) + \frac{1}{2} \mathbf{b}_{-\alpha_{\mu} - \alpha_{\nu}} \cdot f_{\mathbf{k}}^{2,E_2}, \quad (\text{S26}) \end{aligned}$$

$$\begin{aligned} h_{\mu\nu\kappa,\mathbf{k}}^{(3)} &\equiv \left( \hat{\boldsymbol{\phi}}_{\mu} \cdot f_{\mathbf{k}}^{E_2} \right) \left( \hat{\boldsymbol{\phi}}_{\nu} \cdot f_{\mathbf{k}}^{E_2} \right) \left( \hat{\boldsymbol{\phi}}_{\kappa} \cdot f_{\mathbf{k}}^{E_2} \right) \\ &= \frac{1}{4} \left( \mathbf{b}_{-\alpha_{\mu} + \alpha_{\nu} + \alpha_{\kappa}} + \mathbf{b}_{\alpha_{\mu} - \alpha_{\nu} + \alpha_{\kappa}} + \mathbf{b}_{\alpha_{\mu} + \alpha_{\nu} - \alpha_{\kappa}} \right) \cdot f_{\mathbf{k}}^{E_2} \\ &\quad + \frac{1}{4} \cos(\alpha_{\mu} + \alpha_{\nu} + \alpha_{\kappa}) f_{\mathbf{k}}^{A_1} - \frac{1}{4} \sin(\alpha_{\mu} + \alpha_{\nu} + \alpha_{\kappa}) f_{\mathbf{k}}^{A_2}, \quad (\text{S27}) \end{aligned}$$

$$\begin{aligned} h_{\mu\nu\kappa\lambda,\mathbf{k}}^{(4)} &\equiv \left( \hat{\boldsymbol{\phi}}_{\mu} \cdot f_{\mathbf{k}}^{E_2} \right) \left( \hat{\boldsymbol{\phi}}_{\nu} \cdot f_{\mathbf{k}}^{E_2} \right) \left( \hat{\boldsymbol{\phi}}_{\kappa} \cdot f_{\mathbf{k}}^{E_2} \right) \left( \hat{\boldsymbol{\phi}}_{\lambda} \cdot f_{\mathbf{k}}^{E_2} \right) \\ &= \frac{1}{8} \mathbf{b}_{\alpha_{\mu} + \alpha_{\nu} + \alpha_{\kappa} + \alpha_{\lambda}} \cdot f_{\mathbf{k}}^{4,E_2} + \frac{1}{8} \left[ \cos(\alpha_{\mu} + \alpha_{\nu} - \alpha_{\kappa} - \alpha_{\lambda}) \right. \\ &\quad \left. + \cos(\alpha_{\mu} - \alpha_{\nu} + \alpha_{\kappa} - \alpha_{\lambda}) + \cos(\alpha_{\mu} - \alpha_{\nu} - \alpha_{\kappa} + \alpha_{\lambda}) \right] \\ &\quad + \frac{1}{8} \left( \mathbf{b}_{-\alpha_{\mu} - \alpha_{\nu} - \alpha_{\kappa} + \alpha_{\lambda}} + \mathbf{b}_{-\alpha_{\mu} - \alpha_{\nu} + \alpha_{\kappa} - \alpha_{\lambda}} \right. \\ &\quad \left. + \mathbf{b}_{-\alpha_{\mu} + \alpha_{\nu} - \alpha_{\kappa} - \alpha_{\lambda}} + \mathbf{b}_{\alpha_{\mu} - \alpha_{\nu} - \alpha_{\kappa} - \alpha_{\lambda}} \right) \cdot f_{\mathbf{k}}^{2,E_2}. \quad (\text{S28}) \end{aligned}$$

To the fifth and sixth orders, we will only need the diagonal parts  $h_{\mu,\mathbf{k}}^{(l)} = \left( \hat{\boldsymbol{\phi}}_{\mu} \cdot f_{\mathbf{k}}^{E_2} \right)^l$ , given by

$$h_{\mu,\mathbf{k}}^{(5)} = \frac{9}{16} \left( \mathbf{b}_{\alpha_{\mu}} \cdot f_{\mathbf{k}}^{E_2} \right) + h_{\mathbf{k}}^{\text{tri}} \left[ \frac{5}{16} + \frac{1}{8} \left( \mathbf{b}_{-2\alpha_{\mu}} \cdot f_{\mathbf{k}}^{2,E_2} \right) \right], \quad (\text{S29})$$

$$h_{\mu,\mathbf{k}}^{(6)} = \frac{9}{32} + \frac{3}{8} \left( \mathbf{b}_{\alpha_{\mu}} \cdot f_{\mathbf{k}}^{E_2} \right) h_{\mathbf{k}}^{\text{tri}} + \frac{9}{32} \mathbf{b}_{-2\alpha_{\mu}} \cdot f_{\mathbf{k}}^{2,E_2} + \frac{\left( h_{\mathbf{k}}^{\text{tri}} \right)^2}{16}, \quad (\text{S30})$$

where we defined  $h_{\mathbf{k}}^{\text{tri}} = \cos(3\alpha_{\mu}) f_{\mathbf{k}}^{A_1} - \sin(3\alpha_{\mu}) f_{\mathbf{k}}^{A_2}$ .

## A. Single layer

We start by deriving the free energy expansion for a single layer  $\mu$  described by the Hamiltonian (S10). The corresponding electronic Green's function is given by:

$$\hat{\mathcal{G}}^{-1} = \hat{\mathcal{G}}_0^{-1} - \hat{\mathcal{V}}, \quad (\text{S31})$$

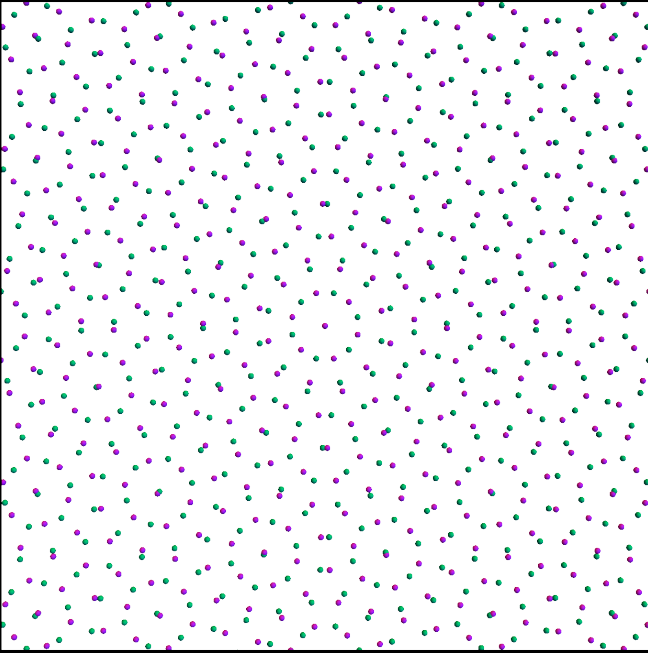


Figure S1. Quasi-crystalline pattern in real space of the  $30^\circ$ -twisted bilayer system. Top-layer sites (purple) and bottom-layer sites (green) can come arbitrarily close to each other, but they are only perfectly aligned at the origin.

where

$$\hat{\mathcal{G}}_{0,k}^{-1} = (i\omega_n - \varepsilon_k - \delta_0 f_k^{A_1}) \sigma^0, \quad \hat{\mathcal{V}}_k = g (\boldsymbol{\phi}_\mu \cdot \mathbf{f}_k^{E_2}) \sigma^0, \quad (\text{S32})$$

denote the bare Green's function and the nematic contribution, respectively. Performing a fermionic Gaussian integration of the corresponding partition function with respect to the electronic degrees of freedom, we obtain the effective bosonic action

$$S_{\text{eff}}[\boldsymbol{\phi}_\mu] = -\text{Tr} \ln(-\beta \hat{\mathcal{G}}^{-1}) + \frac{\boldsymbol{\phi}_\mu^2}{2U_{\text{nem}}}, \quad (\text{S33})$$

where the last term arises from the Hubbard-Stratonovich decoupling of the fermionic interaction term, with  $U_{\text{nem}}$  denoting the interaction projected onto the nematic channel. Expanding the effective action (S33) in terms of the (uniform) order parameter  $\boldsymbol{\phi}_\mu$  leads to the Landau expansion of the free energy, which is given by  $\mathcal{F} = S_{\text{eff}} T$  with  $S_{\text{eff}}$  evaluated at the saddle point. It is convenient to use the relation

$$-\text{Tr} \ln(-\beta \hat{\mathcal{G}}^{-1}) = -\text{Tr} \ln(-\beta \hat{\mathcal{G}}_0^{-1}) + \sum_{l=1}^{\infty} \mathcal{S}^{(l)}, \quad (\text{S34})$$

where

$$\mathcal{S}^{(l)} = \frac{1}{l} \sum_{n,\mathbf{k}} \text{tr}_\sigma \left( \hat{\mathcal{G}}_{0,k} \hat{\mathcal{V}}_k \right)^l = \frac{2}{l} \sum_{n,\mathbf{k}} \frac{g^l}{d_k^l} \left( \boldsymbol{\phi}_\mu \cdot \mathbf{f}_k^{E_2} \right)^l, \quad (\text{S35})$$

and

$$d_k = i\omega_n - \varepsilon_k - \delta_0 f_k^{A_1}. \quad (\text{S36})$$

As explained above, the  $\mathbf{k}$  integral only evaluates to a non-zero value for  $A_1$ -contributions in the decompositions (S26)-(S28). We then obtain the free-energy expansion

$$\mathcal{F}[\boldsymbol{\phi}_\mu] = r |\boldsymbol{\phi}_\mu|^2 + u |\boldsymbol{\phi}_\mu|^4 + \lambda_3 |\boldsymbol{\phi}_\mu|^3 \cos(3\alpha_\mu), \quad (\text{S37})$$

with the coefficients

$$r = \frac{1}{2U_{\text{nem}}} + \frac{g^2 T}{2} \sum_{n,\mathbf{k}} \frac{1}{d_k^2}, \quad u = \frac{3g^4 T}{16} \sum_{n,\mathbf{k}} \frac{1}{d_k^4},$$

$$\lambda_3 = \frac{g^3 T}{6} \sum_{n,\mathbf{k}} \frac{f_k^{A_1}}{d_k^3}. \quad (\text{S38})$$

## B. Twisted bilayer

We now proceed to compute the Landau coefficients of the twisted hexagonal bilayer system given by the total Hamiltonian (S22) for an arbitrary twist angle  $\theta_{\text{tw}}$ . The fermionic Green's function  $\hat{\mathcal{G}}^{-1} = \hat{\mathcal{G}}_0^{-1} - \hat{\mathcal{V}}$  is given by

$$\hat{\mathcal{G}}_{0,k}^{-1} = \left( F_k^{A_1} \tau^0 - F_k^{A_2} \tau^z - t \tau^x \right) \sigma^0, \quad (\text{S39})$$

$$\hat{\mathcal{V}}_k = g \left[ \left( \boldsymbol{\phi}_+ \cdot \mathbf{f}_k^{E_2} \right) \tau^0 + \left( \boldsymbol{\phi}_- \cdot \mathbf{f}_k^{E_2} \right) \tau^z \right] \sigma^0, \quad (\text{S40})$$

where, for brevity, we defined

$$F_k^{A_1} = i\omega_n - \varepsilon_k - \delta_0 f_k^{A_1} \cos(3\theta_{\text{tw}}), \quad F_k^{A_2} = \delta_0 f_k^{A_2} \sin(3\theta_{\text{tw}}). \quad (\text{S41})$$

The nematic order parameter combinations are parameterized by  $\boldsymbol{\phi}_\pm = |\boldsymbol{\phi}_\pm| (\cos \alpha_\pm, \sin \alpha_\pm)$ . Analogous to the previous case, the Gaussian integration generates the effective free energy

$$\mathcal{F}_{\text{eff}} = -T \text{Tr} \ln(-\beta \hat{\mathcal{G}}^{-1}) + \frac{\boldsymbol{\phi}_+^2}{2U_+} + \frac{\boldsymbol{\phi}_-^2}{2U_-}, \quad (\text{S42})$$

where, to keep the approach general, we introduced different effective interactions  $U_\pm$  in each channel, which is allowed by the symmetry of the problem. To expand the trace-log in terms of  $\boldsymbol{\phi}_+$  and  $\boldsymbol{\phi}_-$  we employ Eq. (S34) and evaluate

$$\mathcal{F}^{(l)} = \frac{T}{l} \sum_{n,\mathbf{k}} \text{tr}_{\sigma,\tau} \left( \hat{\mathcal{G}}_{0,k} \hat{\mathcal{V}}_k \right)^l. \quad (\text{S43})$$

Using the symmetry decompositions (S26)-(S30), and the same logic as above, i.e. that only  $A_1$  terms contribute to a non-zero sum, we compute  $\mathcal{F}^{(l)}$  order by order. While the linear term  $\mathcal{F}^{(1)} = 0$  vanishes, the quadratic contribution  $\tilde{\mathcal{F}}^{(2)} \equiv \frac{1}{2} \left( \frac{\boldsymbol{\phi}_+^2}{U_+} + \frac{\boldsymbol{\phi}_-^2}{U_-} \right) + \mathcal{F}^{(2)}$  becomes

$$\tilde{\mathcal{F}}^{(2)} = \frac{\boldsymbol{\phi}_+^2}{2U_+} + \frac{\boldsymbol{\phi}_-^2}{2U_-} + 2g^2 T \sum_{n,\mathbf{k}} \left\{ I_{k,+}^{(2)} (\boldsymbol{\phi}_+ \cdot \mathbf{f}_k^{E_2})^2 \right. \\ \left. + I_{k,-}^{(2)} (\boldsymbol{\phi}_- \cdot \mathbf{f}_k^{E_2})^2 + 4d_k^{-2} F_k^{A_1} F_k^{A_2} (\boldsymbol{\phi}_+ \cdot \mathbf{f}_k^{E_2}) (\boldsymbol{\phi}_- \cdot \mathbf{f}_k^{E_2}) \right\} \\ = r_+ |\boldsymbol{\phi}_+|^2 + r_- |\boldsymbol{\phi}_-|^2, \quad (\text{S44})$$

where we defined the quadratic Landau parameter

$$r_{\pm} = \frac{1}{2U_{\pm}} + g^2 T \sum_{n,k} I_{k,\pm}^{(2)}, \quad (\text{S45})$$

with

$$I_{k,\pm}^{(2)} = \left[ (F_k^{A_1})^2 + (F_k^{A_2})^2 \pm t^2 \right] / d_k^2, \quad (\text{S46})$$

$$d_k = (F_k^{A_1})^2 - (F_k^{A_2})^2 - t^2. \quad (\text{S47})$$

The reason why the two nematic channels  $\phi_{\pm}$  are decoupled on the quadratic level is because the last term in the curly bracket in (S44) vanishes, since the decompositions (S26) have no  $A_2$  contribution.

For the cubic contribution to the free energy, we obtain

$$\begin{aligned} \mathcal{F}^{(3)} = & \lambda_+^{(3c)} c_{3\theta_{\text{tw}}} |\phi_+|^3 c_{3\alpha_+} + 3\lambda_-^{(3c)} c_{3\theta_{\text{tw}}} |\phi_-|^2 |\phi_+| c_{\alpha_+ + 2\alpha_-} \\ & + \lambda_+^{(3s)} s_{3\theta_{\text{tw}}} s_{3\alpha_-} |\phi_-|^3 + \lambda_-^{(3s)} 3s_{3\theta_{\text{tw}}} |\phi_+|^2 |\phi_-| s_{2\alpha_+ + \alpha_-}, \end{aligned} \quad (\text{S48})$$

where we defined  $c_{\gamma} \equiv \cos(\gamma)$  and  $s_{\gamma} \equiv \sin(\gamma)$ , as well as the Landau parameters

$$\lambda_{\pm}^{(3c)} = \frac{g^3 T}{3} \sum_{n,k} \left( \frac{(i\omega_n - \varepsilon_k) f_k^{A_1}}{\cos(3\theta_{\text{tw}})} - \delta_0 (f_k^{A_1})^2 \right) I_{k,\pm}^{(3A)}, \quad (\text{S49})$$

$$\lambda_{\pm}^{(3s)} = -\frac{g^3 T}{3} \sum_{n,k} \delta_0 (f_k^{A_2})^2 I_{k,\pm}^{(3B)}, \quad (\text{S50})$$

and the integrands

$$I_{k,\pm}^{(3A)} = \left[ (F_k^{A_1})^2 + 3(F_k^{A_2})^2 + (1 \pm 2)t^2 \right] / d_k^3, \quad (\text{S51})$$

$$I_{k,\pm}^{(3B)} = \left[ 3(F_k^{A_1})^2 + (F_k^{A_2})^2 - (1 \pm 2)t^2 \right] / d_k^3. \quad (\text{S52})$$

At first sight, it might appear that  $\lambda_{\pm}^{(3c)}$  in Eq. (S49) is singular at  $\theta_{\text{tw}} = \pi/6$ . However, this is not the case. To see this, we symmetrize the first term in (S49) using a  $C_{12z}$  operation upon which  $f_{\mathcal{R}_z(\frac{2\pi}{12})\mathbf{k}}^{A_1, A_2} = -f_{\mathbf{k}}^{A_1, A_2}$ . Then, we find the result

$$\begin{aligned} \frac{(i\omega_n - \varepsilon_k) f_k^{A_1}}{\cos(3\theta_{\text{tw}})} \left[ I_{k,\pm}^{(3A)} - I_{(\omega_n, \mathcal{R}_z(\frac{\pi}{6})\mathbf{k}), \pm}^{(3A)} \right] \\ = \delta_0 (i\omega_n - \varepsilon_k)^2 (f_k^{A_1})^2 \tilde{I}_{k,\pm}^{(3A)}. \end{aligned} \quad (\text{S53})$$

Since  $\tilde{I}_{k,\pm}^{(3A)}$  depends on  $\cos(3\theta_{\text{tw}})$  only in a trivial (analytical) way, this justifies the overall prefactor  $\cos(3\theta_{\text{tw}})$  in Eq. (S48).

For the quartic contribution, we find

$$\mathcal{F}^{(4)} = u_+ |\phi_+|^4 + u_- |\phi_-|^4 + u_3 \left[ \phi_+^2 \phi_-^2 + 2(\phi_+ \cdot \phi_-)^2 \right], \quad (\text{S54})$$

where the Landau parameters are

$$u_{\pm} = \frac{3T}{8} g^4 \sum_{n,k} I_{k,\pm}^{(4A)}, \quad u_3 = \frac{3T}{4} g^4 \sum_{n,k} I_k^{(4B)}, \quad (\text{S55})$$

and the integrands are defined as

$$\begin{aligned} I_{k,\pm}^{(4A)} = \frac{1}{d_k^4} \left\{ d_k^2 + 8(F_k^{A_1})^2 (F_k^{A_2})^2 + 4t^2 (1 \pm 1) (F_k^{A_1})^2 \right. \\ \left. + 4t^2 (-1 \pm 1) (F_k^{A_2})^2 \right\}, \end{aligned} \quad (\text{S56})$$

$$I_k^{(4B)} = \frac{(F_k^{A_1})^4 + (F_k^{A_2})^4 + 6(F_k^{A_1})^2 (F_k^{A_2})^2 - t^4 - \frac{2t^2}{3} d_k}{d_k^4}. \quad (\text{S57})$$

Since the two order parameters are already coupled at the quartic level (S54), for the fifth- and sixth-order terms we only derive the contributions that depend on one of the order parameters. The fifth-order terms becomes

$$\mathcal{F}^{(5)} = u_+^{(5)} c_{3\theta_{\text{tw}}} |\phi_+|^5 c_{3\alpha_+} + u_-^{(5)} s_{3\theta_{\text{tw}}} |\phi_-|^5 s_{3\alpha_-}, \quad (\text{S58})$$

where we used again the notation  $c_{\gamma} \equiv \cos(\gamma)$  and  $s_{\gamma} \equiv \sin(\gamma)$ , and defined the Landau parameters

$$u_+^{(5)} = \frac{T}{2} g^5 \sum_{n,k} \left( \frac{(i\omega_n - \varepsilon_k) f_k^{A_1}}{\cos(3\theta_{\text{tw}})} - \delta_0 (f_k^{A_1})^2 \right) I_{k,+}^{(5)}, \quad (\text{S59})$$

$$u_-^{(5)} = -\frac{T}{2} g^5 \delta_0 \sum_{n,k} (f_k^{A_2})^2 I_{k,-}^{(5)}. \quad (\text{S60})$$

The integrand is given by:

$$\begin{aligned} I_{k,\pm}^{(5)} = \frac{1}{d_k^5} \left\{ \frac{5}{2} \left[ (F_k^{A_1})^2 + (F_k^{A_2})^2 \pm t^2 \right]^2 - (1 \pm 1) (F_k^{A_1})^4 \right. \\ \left. - (1 \mp 1) (F_k^{A_2})^4 \right\}. \end{aligned} \quad (\text{S61})$$

The  $\cos(3\theta_{\text{tw}})$  in the denominator in Eq. (S59) cancels for the same reasons as in relation (S53).

Finally, for the sixth-order we find

$$\mathcal{F}^{(6)} = u_+^{(6)} |\phi_+|^6 + u_-^{(6)} |\phi_-|^6 + \lambda_6^{(+)} |\phi_+|^6 c_{6\alpha_+} + \lambda_6^{(-)} |\phi_-|^6 c_{6\alpha_-}, \quad (\text{S62})$$

with

$$u_{\pm}^{(6)} = \frac{5g^6 T}{12} \sum_{n,k} I_{k,\pm}^{(6)}, \quad (\text{S63})$$

$$\lambda_6^{(\pm)} = \frac{g^6 T}{24} \sum_{n,k} \left[ (f_k^{A_1})^2 - (f_k^{A_2})^2 \right] I_{k,\pm}^{(6)}, \quad (\text{S64})$$

as well as

$$I_{k,\pm}^{(6)} = \frac{1}{2d_k^3} + \frac{(F_k^{A_2})^2 + \frac{1 \pm 1}{2} t^2}{d_k^6} \left[ 3(F_k^{A_1})^2 + (F_k^{A_2})^2 - (1 \mp 2)t^2 \right]^2. \quad (\text{S65})$$

### III. SPECTRAL FUNCTION AND PSEUDOGAP-LIKE BEHAVIOR IN THE CRITICAL PHASE

Here we present details of the evaluation of the one-loop fermionic self-energy. As shown in the main text, in the critical

region where the fermions couple to the nematic fluctuations, it is given by

$$\Sigma(\omega, \mathbf{k}) = g^2 A_0 T \sum_{ij} \int_{\mathbf{q}} \chi_{\text{nem}}^{ij}(\Omega, \mathbf{q}) f_{\mathbf{k}-\frac{\mathbf{q}}{2}}^{E_2} f_{\mathbf{k}-\frac{\mathbf{q}}{2}, j}^{E_2} \mathcal{G}(\omega - \Omega, \mathbf{k} - \mathbf{q}) \quad (\text{S66})$$

Throughout this section, we set both Planck and Boltzmann's constants to be  $\hbar = k_B = 1$ . We focus on the contributions of the fermions at the Fermi level, with momenta  $\mathbf{k}_F \equiv |\mathbf{k}_F(\theta)|(\cos\theta, \sin\theta)$ , and for simplicity, we assume a spherical Fermi surface where  $|\mathbf{k}_F(\theta)| = k_F = \text{const}$ . To keep the discussion general, for the non-interacting fermionic propagator we use a linearized dispersion and a finite lifetime  $\tau_0$ :

$$\mathcal{G}^{-1}(\omega, \mathbf{k}_F - \mathbf{q}) = \omega - \mathbf{v}_F \cdot \mathbf{q} + \frac{i}{2\tau_0}, \quad (\text{S67})$$

where  $\mathbf{v}_F = \mathbf{k}_F/m$  is the Fermi velocity. We also neglect the  $\mathbf{q}$  dependence of the vertex function, which becomes  $\mathbf{f}_{\mathbf{k}-\frac{\mathbf{q}}{2}}^{E_2} \approx \mathbf{f}_{\mathbf{k}}^{E_2} = (\cos 2\theta, -\sin 2\theta)$ . Moreover, since we are interested in the thermal transition, we set the bosonic Matsubara frequency to zero and write the bosonic propagator as

$$\chi_{\text{nem}}^{ij}(0, \mathbf{q}) = (|\mathbf{q}|/k_F)^{\eta-2} \delta_{ij} \chi_0, \quad (\text{S68})$$

where  $\eta$  is the anomalous exponent characterizing the critical phase, and the prefactor  $\chi_0$  has dimensions of (energy) $^{-1}$ .

Using all of the above ingredients, the self-energy is given by:

$$\Sigma(\omega, \mathbf{k}_F) = \int \frac{d\mathbf{q}}{(2\pi)^2} \frac{g^2 \chi_0 A_0 T}{\left(\frac{|\mathbf{q}|}{k_F}\right)^{2-\eta} \left(\omega - \mathbf{v}_F \cdot \mathbf{q} + \frac{i}{2\tau_0}\right)}. \quad (\text{S69})$$

We perform a change of variables to dimensionless Cartesian coordinates  $(x, y)$  where  $x$  is the momentum  $\mathbf{q}$  in units of  $k_F$  along the direction transverse to the Fermi surface, and  $y$  is the momentum  $\mathbf{q}$  in units of  $k_F$  along the direction longitudinal to the Fermi surface. We obtain

$$\Sigma(\omega, \mathbf{k}_F) = \int_{-\infty}^{\infty} \int_{-\infty}^{\infty} \frac{\kappa T dx dy}{(x^2 + y^2)^{1-\frac{\eta}{2}} \left(\frac{\omega}{E_F} - 2x + \frac{i}{2E_F\tau_0}\right)}, \quad (\text{S70})$$

where  $E_F = k_F^2/2m$  is the Fermi energy and  $\kappa$  is a dimensionless parameter given by  $\kappa = \frac{g^2 k_F^2 A_0 \chi_0}{(2\pi)^2 E_F}$ . Evaluating the integral, we obtain the analytical expression:

$$\Sigma(\omega, \mathbf{k}_F) = \kappa T c_\eta e^{-i\frac{\eta\pi}{2}} \left(\frac{2\omega\tau_0 + i}{2E_F\tau_0}\right)^{\eta-1}, \quad (\text{S71})$$

where we defined  $c_\eta$  as

$$c_\eta = \frac{\pi^{\frac{3}{2}} \Gamma\left(\frac{1}{2} - \frac{\eta}{2}\right)}{2^\eta \Gamma\left(1 - \frac{\eta}{2}\right)} \frac{1}{\sin\left(\frac{\eta\pi}{2}\right)}, \quad (\text{S72})$$

and  $\Gamma(x)$  is the Gamma function. The coefficient  $c_\eta$  varies smoothly in the range  $[26.6, 57.2]$  for the allowed values of  $\eta \in [1/9, 1/4]$ . The real and imaginary parts of the spectral function are given by

$$\text{Re} \Sigma(\omega, \mathbf{k}_F) = \text{sgn}(\omega) \Sigma_0 \cos(\gamma), \quad \text{Im} \Sigma(\omega, \mathbf{k}_F) = \Sigma_0 \sin(\gamma), \quad (\text{S73})$$

with magnitude and phase

$$\Sigma_0 = \kappa T c_\eta \left(\frac{4\omega^2 \tau_0^2 + 1}{4E_F^2 \tau_0^2}\right)^{\frac{\eta-1}{2}}, \quad (\text{S74})$$

$$\gamma = (\eta - 1) \arctan\left(\frac{1}{2|\omega|\tau_0}\right) - \frac{\eta\pi}{2}. \quad (\text{S75})$$

We can now compute the spectral function  $A(\omega, \mathbf{k}_F) = -2\text{Im}[\hat{\mathcal{G}}(\omega, \mathbf{k}_F)]$ , where  $\hat{\mathcal{G}}^{-1} = \mathcal{G}^{-1} - \Sigma$  is the renormalized Green's function. The resulting function,

$$A(\omega, \mathbf{k}_F) = \frac{-2\text{Im} \Sigma(\omega, \mathbf{k}_F)}{[\omega - \text{Re} \Sigma(\omega, \mathbf{k}_F)]^2 + [\text{Im} \Sigma(\omega, \mathbf{k}_F)]^2}, \quad (\text{S76})$$

is plotted in Fig. 3 of the main text for  $T = 0.01 E_F$ ,  $\tau_0 = 50 E_F^{-1}$ ,  $\kappa = 0.02$  and  $\eta \in [0.1, 0.25]$ . The pseudogap-like energy scale set by the distance between the peaks of the spectral function can be obtained analytically in the limit  $\tau_0 \rightarrow \infty$ :

$$\Sigma_0 = \kappa T c_\eta \left(\frac{|\omega|}{E_F}\right)^{\eta-1}, \quad \gamma = -\frac{\eta\pi}{2}. \quad (\text{S77})$$

Inserting the above expressions into the definition of the spectral function in Eq. (S76) and taking the derivative with respect to  $\omega$ , we find the following condition for the maximum at positive  $\omega$ ,

$$X^2 - 2\kappa a_\eta \frac{2\eta-1}{\eta+1} \frac{T}{E_F} X + 3\kappa^2 c_\eta^2 \frac{\eta-1}{\eta+1} \frac{T^2}{E_F^2} = 0 \quad (\text{S78})$$

where we have defined  $X \equiv (\omega/E_F)^{2-\eta}$  and  $a_\eta \equiv c_\eta \cos\left(\frac{\eta\pi}{2}\right)$ . The positive root of this polynomial gives the position of the maximum,  $\omega_{\text{max}}$ . The value of  $\Delta = 2\omega_{\text{max}}$  is then given by:

$$\Delta \approx 2E_F \left[ \frac{\kappa T}{E_F} \frac{a_\eta (1-2\eta)}{\eta+1} \left( \sqrt{1 + \frac{3c_\eta^2 (1-\eta^2)}{a_\eta^2 (1-2\eta)}} - 1 \right) \right]^{\frac{1}{2-\eta}}. \quad (\text{S79})$$

The pseudogap-like energy scale  $\Delta$  is plotted in Fig. 3(b) of the main text for different values of the lifetime  $\tau_0$ . Clearly, the dependence on  $\tau_0$  is very weak.